Nuclear Science and Techniques (2026) 37:69
https://doi.org/10.1007/s41365-025-01880-4

Systematic study of laser-assisted cluster radioactivity for deformed nuclei

Leng-Jun Liao[1] · Lin-Jing Qi[2] · Xi-Jun Wu[3] · Xiao-Hua Li[1,4,5,6] · Ming Li[1]

Received: 16 May 2025 / Revised: 12 July 2025 / Accepted: 14 July 2025 / Published online: 31 January 2026

Abstract
In this study, the effects of laser fields that can be achieved in the near future on cluster penetration probability and half-life are quantitatively investigated. The calculation results show that extreme laser fields can slightly change the cluster-decay half-life by affecting the penetration probability within a narrow range. Subsequently, we discuss the correlation between the change rate of the penetration probability and the tunneling path. The results indicate that for different parent nuclei emitting the same cluster, nuclei with longer tunneling paths are more easily affected by the laser fields. The shell effect on this correlation is also observed. In addition, the impact of laser fields on the penetration probability in any direction is investigated.

Keywords Cluster radioactivity · Half-life · Extreme laser field · Penetration probability

1 Introduction

Laser is emitted through a process of stimulated emission, in which the electrons of atoms transition from the high-energy state to the low-energy state, releasing coherent photons with a single frequency and forming a laser beam. In the 1960s, American physicist Theodore Maiman successfully constructed the first laser using a ruby crystal as the active medium, which is also known as the Maiman laser [1]. Because the experimental intensities of lasers are insufficient to directly excite the atomic nucleus and the available photon energies are lower than the characteristic energies of nuclear transitions, the induction of nuclear processes through laser interactions has long been considered impossible. However, with the continuous advancement of experimental laser technology, the laser energy and peak intensity have recently improved significantly. To date, the peak intensity of laser pulses has reached 1×10^{23} W/cm^2 [2]. The laser electric field strength corresponding to this intensity is comparable to the Coulomb field strength from the atomic nucleus at a distance of approximately 10 fm [3–5]. In the near future,

This work was supported in part by the National Natural Science Foundation of China (Nos. 12175100 and 11975132), the Construct Program of the Key Discipline in Hunan Province, the Research Foundation of Education Bureau of Hunan Province, China (Nos. 21B0402, 18A237, and 22A0305), the Natural Science Foundation of Hunan Province, China (No. 2018JJ2321), the Innovation Group of Nuclear and Particle Physics in USC, the Shandong Province Natural Science Foundation, China (No. ZR2022JQ04) and the Opening Project of Cooperative Innovation Center for Nuclear Fuel Cycle Technology and Equipment, University of South China (No. 2019KFZ10), and the Hunan Provincial Innovation Foundation for Postgraduate (No. CX20251453).

✉ Xi-Jun Wu
wuxijun1980@yahoo.cn

✉ Xiao-Hua Li
lixiaohuaphysics@126.com

✉ Ming Li
liming1631223@163.com

[1] School of Nuclear Science and Technology, University of South China, Hengyang 421001, China

[2] School of Physics and Astronomy, Beijing Normal University, Beijing 100875, China

[3] School of Math and Physics, University of South China, Hengyang 421001, China

[4] Key Laboratory of Advanced Nuclear Energy Design and Safety, Ministry of Education, Hengyang 421001, China

[5] Cooperative Innovation Center for Nuclear Fuel Cycle Technology and Equipment, University of South China, Hengyang 421001, China

[6] National Exemplary Base for International Science and Technology Collaboration of Nuclear Energy and Nuclear Safety, University of South China, Hengyang 421001, China

the Extreme Light Infrastructure for Nuclear Physics (ELI-NP) and Shanghai Superintense Ultrafast Laser Facility (SULF) are expected to increase laser intensity by one or two orders of magnitude [6–8]. These developments provide a unique opportunity for laser–nuclear interaction studies. Experimentally, Shvyd'ko et al. used an X-ray free-electron laser to perform resonant X-ray excitation on the ^{45}Sc isotope [9]. The uncertainty in the transition energy they determined was two orders of magnitude smaller than that previously reported. Theoretically, many studies have shown that these extreme laser fields not only affect atomic and molecular processes, but also influence nuclear processes. For instance, recent theoretical studies reported that extreme laser fields can excite ^{229}Th to isomeric state through electron recollision [3, 10, 11]. Furthermore, it can affect the half-life of proton radioactivity [12–14] and α decay [15–19] by altering the Coulomb barrier. Nevertheless, as an important decay mode, the influence of extreme laser fields on cluster radioactivity remains to be explored in detail.

Spontaneous nuclear radioactivity has long been regarded as an important channel for exploring the nuclear structures of heavy and superheavy nuclei [20–22]. As one of the main decay modes of superheavy nuclei, cluster radioactivity has received considerable attention in the contemporary nuclear physics community [23–27]. It was first predicted in 1980 by Săndulescu, Poenaru, and Greiner [28] and was first observed in the emission of ^{14}C from a ^{223}Ra probe by Rose and Jones in 1984 [29]. This process is an intermediate process between α decay and spontaneous fission, where the parent nucleus emits a cluster particle that is heavier than an α particle but lighter than the lightest fission fragment, while decaying into a doubly magic daughter nucleus ^{208}Pb or its neighboring daughter nucleus [30, 31]. Exploring the effects of extreme laser fields on cluster radioactivity can provide a new perspective for understanding the interactions between laser fields and nuclear decay processes.

In the present work, considering the preformation probability S_c as well as the deformation of the emitted cluster, we quantitatively investigate the influence of the extreme laser field on cluster-decay half-life and penetration probability. The results indicate that the cluster penetration probability and half-life can be modified by laser fields that can be achieved in the near future to a finite extent. In the calculation of the cluster-decay half-life, the cluster preformation probability S_c plays an important role [32–34]. Different models treat this in various ways. For instance, in fission-like models, S_c is considered the penetrability of the inner part of the barrier for the overlapping region [35]. In the unified fission model (UFM), S_c is generally considered to be unity [36]. However, because the emitted cluster particles within the entire cluster family are completely $N \neq Z$ systems, as a cluster aggregates more nucleons, its likelihood of existing in the parent nucleus decreases [32]. Thus, a reasonable method should be used to calculate S_c rather than simply assuming it to be 1. Considering the impact of nuclear deformation is essential, as the interaction between lasers and nuclei introduces a new electric dipole term in the nuclear Hamiltonian, which is strongly dependent on the angle between the laser field and the emission direction of the cluster. The relationship between the change rate of the penetration probability and tunneling path was subsequently studied. The results show that for different parent nuclei emitting the same cluster, nuclei that provide a longer tunneling path are more easily affected by laser fields. In addition, we found that this relationship was influenced by the shell effect. The impact of laser fields on the cluster penetration probability in any direction is also presented.

The remainder of this paper is organized as follows: A detailed theoretical framework for calculating the cluster-decay half-life in high-intensity laser fields is provided in Sect. 2. The detailed numerical results and discussion are presented in Sect. 3. A simple summary is provided in Sect. 4.

2 Theoretical framework

2.1 The theoretical method

2.1.1 Half-life for the cluster radioactivity

The half-life for the cluster radioactivity can be expressed as [37]

$$T_{1/2} = \frac{\ln 2}{\lambda}. \tag{1}$$

Here, λ is the decay constant that depends on the assault frequency ν, cluster preformation probability S_c and penetration probability P. It can be given by [38]

$$\lambda = \nu P S_c. \tag{2}$$

The oscillation frequency ν is expressed as [39]

$$\nu = \frac{\pi\hbar}{2\mu R_{in}^2}, \tag{3}$$

where $\hbar$ is the reduced Planck constant. $\mu = \frac{M_d M_c}{M_d + M_c}$ is the reduced mass of the emitted cluster–daughter nucleus system with M_d and M_c being the daughter nucleus, and the emitted cluster mass, respectively. $R_{in} = C_c + C_d$ [32] is the saddle point for the touching configuration with $C_i = R_i\left(1 - \frac{b^2}{R_i^2}\right)(i = c, d)$ being the Süssmann central radii [40] of the cluster and daughter nucleus, respectively. The diffuseness parameter of the nuclear surface $b = 1$ fm was

taken from Ref. [41]. The sharp radius R_i can be given as [42]

$$R_i = 1.28A_i^{1/3} - 0.76 + 0.8A_i^{-1/3}, \tag{4}$$

where A_i $(i = \mathrm{c}, \mathrm{d})$ is the mass number of the emitted cluster and daughter nucleus, respectively.

Because the daughter nucleus for cluster radioactivity is often the doubly magic nucleus ^{208}Pb or a nucleus in its neighborhood, which exhibits a spherical or near-spherical shape, we only considered the deformation effect of the emitted cluster in this study. The total penetration probability P was determined by averaging P_φ in all directions. They can be defined as

$$P = \frac{1}{2}\int_0^\pi P_\varphi \sin\varphi \mathrm{d}\varphi, \tag{5}$$

$$P_\varphi = \exp\left[-\frac{2\sqrt{2\mu}}{\hbar}\int_{R_{\mathrm{in}}}^{R_{\mathrm{out}}}\sqrt{V(r,\varphi,t,\theta)-Q_{\mathrm{c}}}\mathrm{d}r\right], \tag{6}$$

where φ represents the orientation angle of the symmetry axis of the deformed cluster. θ denotes the angle between the direction of the laser electric field and that of the emitted cluster. The outer turning point R_{out} of the barrier is obtained by the condition $V(R_{\mathrm{out}}) = Q_{\mathrm{c}}$ [43] with Q_{c} being the cluster radioactivity released energy. It can be given by

$$Q_{\mathrm{c}} = B(A_{\mathrm{c}}, Z_{\mathrm{c}}) + B(A_{\mathrm{d}}, Z_{\mathrm{d}}) - B(A, Z), \tag{7}$$

where $B(A_{\mathrm{c}}, Z_{\mathrm{c}})$, $B(A_{\mathrm{d}}, Z_{\mathrm{d}})$, and $B(A, Z)$ are the binding energies of the emitted cluster, daughter, and parent nuclei, respectively, taken from AME2020 [44] and NUBASE2020 [45], respectively. A is the mass number of the parent nucleus. Z_{c}, Z_{d}, and Z represent the number of protons in the emitted cluster, daughter, and parent nuclei, respectively. The total interaction potential between the emitted cluster and daughter nucleus, as shown in Eq. (6), can be expressed as

$$V(r,\varphi,t,\theta) = V_{\mathrm{N}}(r,\varphi) + V_{\mathrm{C}}(r,\varphi) + V_{\mathrm{l}}(r) + V_{\mathrm{I}}(r,t,\theta). \tag{8}$$

Here, $V_{\mathrm{N}}(r,\varphi)$, $V_{\mathrm{C}}(r,\varphi)$, and $V_{\mathrm{l}}(r)$ correspond to the nuclear, Coulomb, and centrifugal potentials, respectively, and $V_{\mathrm{I}}(r,t,\theta)$ is the interaction of the decaying system with the laser field. A detailed explanation of this interaction is provided in the following section.

In the present work, we choose $V_{\mathrm{N}}(r,\varphi)$ as the classic Woods–Saxon form [46], and it is approximated as the axial deformation, which can be given by:

$$V_{\mathrm{N}}(r,\varphi) = \frac{V_0}{1+\exp\left[\frac{r-R(\varphi)}{a}\right]}, \tag{9}$$

with

$$R(\varphi) = -1.37 + r_{\mathrm{d}} + r_{\mathrm{c}}\left[1 + \beta_2 Y_{20}(\varphi) + \beta_4 Y_{40}(\varphi) + \beta_6 Y_{60}(\varphi)\right]. \tag{10}$$

Here, $Y_{lm}(\varphi)$ represents the spherical harmonic function. β_2, β_4, and β_6 refer to the quadrupole, hexadecapole, and hexacontatetrapole deformations of the emitted cluster, respectively. These were obtained from FRDM2012 [47]. $r_i = 1.27A_i^{1/3}(i = \mathrm{c}, \mathrm{d})$ are the nuclear charge radii. The potential depth V_0 and diffuseness a are parameterized as [46]

$$V_0 = -44.16[1 - 0.4(I_{\mathrm{d}} + I_{\mathrm{c}})]\frac{A_{\mathrm{d}}^{1/3}A_{\mathrm{c}}^{1/3}}{A_{\mathrm{d}}^{1/3} + A_{\mathrm{c}}^{1/3}}, \tag{11}$$

$$a = 0.5 + 0.33I_{\mathrm{d}}, \tag{12}$$

where $I_i = \frac{N_i - Z_i}{A_i}$ $(i = \mathrm{c}, \mathrm{d})$ are the relative neutron excesses of the emitted cluster and daughter nucleus, with N_i $(i = \mathrm{c}, \mathrm{d})$ being the neutron numbers of the emitted cluster and daughter nuclei, respectively.

The Coulomb potential between the daughter nucleus and the deformed cluster can be given as [48, 49]

$$V_{\mathrm{C}}(r,\varphi) = \frac{Z_{\mathrm{c}}Z_{\mathrm{d}}e^2}{r} + 3Z_{\mathrm{c}}Z_{\mathrm{d}}e^2\sum_\lambda \frac{1}{2\lambda+1} \times \frac{R^\lambda(\varphi)}{r^{\lambda+1}}Y_{\lambda 0}(\varphi)\left[\beta_\lambda + \frac{4}{7}\beta_\lambda^2 Y_{\lambda 0}(\varphi)\right]. \tag{13}$$

The centrifugal potential is adopted as the Langer-modified form because $l(l+1) \to (l+\frac{1}{2})^2$ is a necessary correction for one-dimensional problems [38]. It can be expressed as:

$$V_l(r) = \frac{\hbar^2(l+\frac{1}{2})^2}{2\mu r^2}, \tag{14}$$

where l is the orbital angular momentum of the emitted cluster. It is determined by the spin–parity conservation rule and can be given as [24]

$$l = \begin{cases} \triangle_j & \text{for even } \triangle_j \text{ and } \pi = \pi_{\mathrm{d}}, \\ \triangle_j + 1 & \text{for even } \triangle_j \text{ and } \pi \neq \pi_{\mathrm{d}}, \\ \triangle_j & \text{for odd } \triangle_j \text{ and } \pi \neq \pi_{\mathrm{d}}, \\ \triangle_j + 1 & \text{for odd } \triangle_j \text{ and } \pi = \pi_{\mathrm{d}}, \end{cases} \tag{15}$$

where $\triangle_j = |j - j_{\mathrm{d}} - j_{\mathrm{c}}|$. j, π, j_{d}, π_{d}, and j_{c}, π_{c} denote the spin and parity values of the parent nucleus, daughter nucleus, and emitted cluster, respectively.

For the cluster preformation probability S_{c}, when $A_{\mathrm{c}} < 28$, it is calculated by utilizing the exponential relationship between it and the α decay preformation probability, which is expressed as [50]

$$S_c = [S_\alpha]^{\frac{(A_c-1)}{3}}. \tag{16}$$

Here, S_α is obtained from the cluster formation model (CFM), whose detailed information will be presented in the following subsection. For $A_c \geq 28$, the logarithmic form of S_c no longer holds a good linear relationship with the mass number of the emitted cluster, manifesting as a pronounced curvature in the curve, and the slope gradually decreases with the increase in the mass number of the emitted cluster [51]. This indicates that the exponential relationship between S_c and S_α does not hold. Thus, when $A_c \geq 28$, S_c is calculated using the empirical formula proposed by Ren et al. [27]. It can be given as:

$$\log_{10} S_c = \begin{cases} -(0.01674 Z_c Z_d - 2.035466), \\ \text{for even-even nuclei,} \\ -(0.01674 Z_c Z_d - 2.035466) - 1.175, \\ \text{for odd-}A\text{ nuclei.} \end{cases} \tag{17}$$

2.1.2 Cluster-formation model

Within the framework of the CFM, the total initial clusterization state Ψ of the emitted cluster–daughter nucleus system is assumed to be a linear superposition of all its n possible clusterization states Ψ_i [52]. It can be defined as:

$$\Psi = \sum_{i=1}^{n} a_i \Psi_i, \tag{18}$$

$$a_i = \int \Psi_i^* \Psi \mathrm{d}\tau, \tag{19}$$

where a_i represents the superposition coefficient of Ψ_i, which satisfies the orthogonality condition [53],

$$\sum_{i=1}^{n} |a_i|^2 = 1. \tag{20}$$

Similarly, the total wave function is an eigenfunction of Hamiltonian H. It can be expressed as [54]

$$H = \sum_{i=1}^{n} H_i, \tag{21}$$

where H_i is the Hamiltonian for the i-th clusterization state Ψ_i. On account of all the clusterizations describing the same emitted cluster–daughter nucleus system are assumed as sharing the same total energy E_s of the total wavefunction [53], it can be given by:

$$E_s = \sum_{i=1}^{n} |a_i|^2 E_s = \sum_{i=1}^{n} E_{fi}. \tag{22}$$

Here, E_{fi} denotes the formation energy of the cluster in the i-th clusterization state Ψ_i. Thus, the α preformation factor can be given as [54, 55]

$$S_\alpha = |a_\alpha|^2 = \frac{E_{f\alpha}}{E_s}, \tag{23}$$

where a_α and $E_{f\alpha}$ denote the coefficient of the α clusterization state and the formation energy of the α cluster, respectively. In CFM, the α cluster formation energy $E_{f\alpha}$ and total energy of the considered system E_s can be classified into four different cases using the following expressions [53, 56].

Case I for even–even nuclei,

$$\begin{aligned} E_{f\alpha} =& 3B(A,Z) + B(A-4,Z-2) \\ & - 2B(A-1,Z-1) - 2B(A-1,Z), \end{aligned} \tag{24}$$

$$E_s = B(A,Z) - B(A-4,Z-2). \tag{25}$$

Case II for even Z–odd N, i.e., even–odd nuclei,

$$\begin{aligned} E_{f\alpha} =& 3B(A-1,Z) + B(A-5,Z-2) \\ & - 2B(A-2,Z-1) - 2B(A-2,Z), \end{aligned} \tag{26}$$

$$E_s = B(A,Z) - B(A-5,Z-2). \tag{27}$$

Case III for odd Z–even N, i.e. odd–even nuclei,

$$\begin{aligned} E_{f\alpha} =& 3B(A-1,Z-1) + B(A-5,Z-3) \\ & - 2B(A-2,Z-2) - 2B(A-2,Z-1), \end{aligned} \tag{28}$$

$$E_s = B(A,Z) - B(A-5,Z-3). \tag{29}$$

Case IV for doubly-odd nuclei,

$$\begin{aligned} E_{f\alpha} =& 3B(A-2,Z-1) + B(A-6,Z-3) \\ & - 2B(A-3,Z-2) - 2B(A-3,Z-1), \end{aligned} \tag{30}$$

$$E_s = B(A,Z) - B(A-6,Z-3). \tag{31}$$

2.2 The quasistatic condition

Currently, based on the chirped pulse amplification technique, a laser pulse with a peak intensity exceeding 1×10^{23} W/cm^2 can be achieved in the laboratory, with a full width at half maximum (FWHM) of approximately 19.6 fs ($=1.96 \times 10^{-14}$ s) [2]. The laser cycles generated by a near-infrared laser with a pulse wavelength of approximately 800 nm and an X-ray free-electron laser [57] with a photon energy of 10 keV are approximately 10^{-15} s and 10^{-19} s, respectively. In the process of cluster radioactivity, the emitted cluster moves back and forth within the parent nucleus at a certain speed before it penetrates the barrier. Because the

length of the tunnel path is less than 100 fm, we can estimate that the time required for it to pass through the tunnel is less than 10^{-20} s. This is much shorter than the optical cycle of the currently achievable highest-peak-intensity laser pulse. In this case, the process of the emitted cluster penetrating the barrier is regarded as quasistatic, and the variation in the laser field can be neglected.

Additionally, the kinetic energy of the emitted clusters is less than 100 MeV, and the velocity of the emitted clusters in vacuum is much slower than the speed of light. This indicates that the influence of the laser electric field on the emitted clusters was much greater than that of the laser magnetic field. Therefore, we ignored the magnetic component of the laser field in this study.

2.3 Laser–nucleus interaction

The interaction potential between the laser electric field and the nucleus reads [58]

$$V_1(r,t,\theta) = -Z_{\text{eff}}\vec{r}\cdot\vec{\varepsilon}(t) = -Z_{\text{eff}}r\varepsilon(t)\cos\theta, \tag{32}$$

where Z_{eff} is the effective charge for the relative motion. It describes the tendency of the laser electric field to separate the emitted cluster from daughter nucleus and can be expressed as

$$Z_{\text{eff}} = \frac{Z_{\text{c}}A_{\text{d}} - Z_{\text{d}}A_{\text{c}}}{A_{\text{d}} + A_{\text{c}}}. \tag{33}$$

Here, $Z_i\,(i = \text{c}, \text{d})$ denotes the proton number of the emitted cluster and daughter nucleus, respectively.

In the present work, the electric component of the laser pulse is chosen to be a linearly polarized Gaussian plane waveforms. It is given as

$$\varepsilon(t) = \varepsilon_0 f(t)\sin(\omega t), \tag{34}$$

where ω is the angular frequency of the wave. The peak of the laser electric field is interrelated with the peak intensity of the laser I_0. It is defined as [12]

$$\varepsilon_0[\text{MV}\cdot\text{fm}^{-1}] = 27.44\times10^{-19}(I_0[\text{W}\cdot\text{cm}^{-2}])^{1/2}. \tag{35}$$

The envelope function of temporal profile can be expressed as:

$$f(t) = \exp\left(-\frac{t^2}{\tau^2}\right). \tag{36}$$

Here, $\tau = xT_0$ is the pulse width of the envelope, with T_0 being the pulse period.

In extreme laser field environments, it is essential to consider the influence of the laser electric field on the decay energy. The change in decay energy is equal to the energy gained by the emitted cluster as it is accelerated by the laser electric field while penetrating the potential barrier. The decay energy of the emitted cluster, considering the laser electric field impact, can be expressed as:

$$Q_{\text{c}}^{*} = Q_{\text{c}} + eZ_{\text{c}}\varepsilon(t)R(\varphi)\cos\theta. \tag{37}$$

3 Results and discussion

Based on the high-intensity laser pulses expected to be achieved by ELI-NP and SULF in the forthcoming years, we quantitatively investigated the impact of the extreme laser fields on cluster radioactivity. To display the effect of the laser electric field on the cluster-decay half-life, we define this effect as the rate of relative change of half-life and express it as

$$\Delta T = \frac{T(\varepsilon,\theta) - T(\varepsilon=0)}{T(\varepsilon=0)}. \tag{38}$$

Here, $T(\varepsilon,\theta)$ and $T(\varepsilon=0)$ represent the cluster-decay half-lives with and without considering the laser electric field, respectively. Based on the Wentzel–Kramers–Brillouin approximation [25] and considering the effect of cluster deformation and the cluster preformation probability, we calculate the half-lives of 26 trans-lead nuclei without taking into account the laser electric field. The detailed results are presented in Table 1. In this table, the first three columns refer to the processes of cluster radioactivity, the angular momentum l carried away by the emitted cluster, and the cluster radioactivity decay energy Q_{c}, respectively. The following three columns are the quadrupole β_2, hexadecapole β_4, and hexacontatetrapole β_6 deformation parameters for the emitted cluster. The last two columns correspond to the logarithmic form of the experimental half-lives and the theoretical half-lives calculated by our theoretical model, respectively. The experimental data on the cluster-decay half-lives were taken from Refs. [23, 26, 46, 59]. From this table, it is clear that the calculated results are in agreement with the experimental data. For a more intuitive comparison, the discrepancies between the theoretical half-lives and experimental data are plotted in Fig. 1. As can be seen from this figure, the differences between the calculated results from our model and the experimental data are within or near ±1. To further investigate these differences, the standard deviation σ was used. It is given by:

$$\sigma = \sqrt{\frac{1}{n}\sum_{i=1}^{n}(\log_{10}T_{1/2}^{\text{cal},i} - \log_{10}T_{1/2}^{\text{exp},i})^2}, \tag{39}$$

where $\log_{10}T_{1/2}^{\text{cal},i}$ and $\log_{10}T_{1/2}^{\text{exp},i}$ refer to the logarithmic form of the theoretical and experimental half-lives for the i-th nucleus, respectively. n is the number of nuclei. Based on

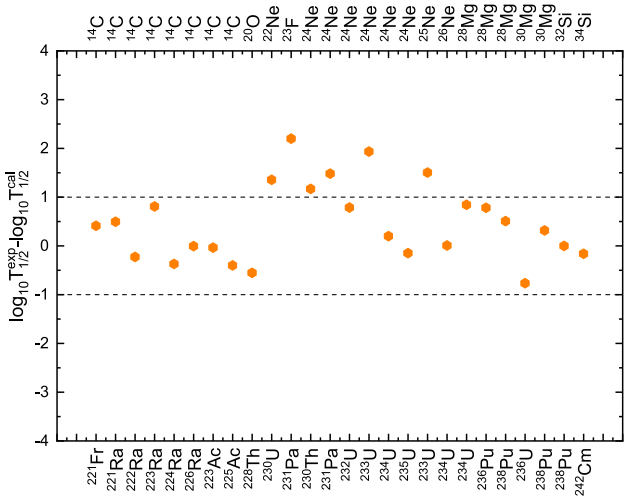

Fig. 1 (Color online) The discrepancy between the calculated values of cluster-decay half-life logarithm and the experimental data. The lower isotope symbols represent the parent nuclei, while the upper isotope symbols denote the corresponding emitted cluster

Eq. (39), we can obtain $\sigma = 0.898$. This indicates that the theoretical half-lives can reproduce the experimental data well and that our model is reliable.

Because the emitted cluster collides with the potential barrier inside the nucleus, the collision frequency ν is insensitive to the external laser field. This suggests that the external laser field primarily affects the cluster-decay half-life by altering the penetration probability. The rate of relative change of penetration probability is defined as:

$$\Delta P = \frac{P(\varepsilon,\theta) - P(\varepsilon = 0)}{P(\varepsilon = 0)}, \tag{40}$$

where $P(\varepsilon,\theta)$ and $P(\varepsilon = 0)$ denote the cluster penetration probabilities with and without considering the laser electric field, respectively.

Based on Eq. (38) and (40), we calculated the influence of laser fields with an intensity of 1×10^{24} W/cm^2 on the cluster penetration probability and half-life when the laser electric field was aligned with the emission direction of the cluster. The detailed results are presented in Table 2. The labels of the first three columns are similar to those in Table 1. The fourth column represents the average tunneling path length $|R| = \frac{1}{\pi}\int_0^{\pi}(R_{\text{out}}(\varphi) - R_{\text{in}})\mathrm{d}\varphi$. The fifth and sixth columns indicate the relative change rates of the cluster penetration probability and half-life, respectively, at an intensity of 1×10^{24} W/cm^2. As can be observed from this table, for most parent nuclei, the laser fields cause slight changes in the cluster penetration probability and half-life, and the rate of change ranges from 0.067% to 0.115%. ^{238}Pu exhibits the highest sensitivity to laser electric fields. Moreover, we find from Table 2 that for different parent nuclei emitting the same clusters, the cluster radioactive nuclei that provide longer tunneling paths are more easily modified by external laser fields. To more intuitively observe this phenomenon, we plot the relationship between ΔP and the tunneling path for the cluster emissions of ^{14}C from Ra, ^{24}Ne from U and ^{28}Mg from Pu isotopes in Fig. 2. As shown, for the emission of the same cluster, ΔP increases as $|R|$ increases. This is attributable to the fact that nuclei with longer tunneling path length possess greater potential barrier widths, leading to lower penetration probability. When a laser field is applied, the reduction in the barrier height or modifications to the barrier shape exert a more pronounced effect on enhancing the penetration probability. Because of the unobservability of the tunneling path in the experiment, we used the observable decay width to replace it for illustration. For different parent nuclei emitting the same cluster, a lower decay width usually leads to a longer tunneling path for cluster radioactivity. This implies that using cluster radioactive nuclei with a lower decay width can result in a more pronounced rate of change of in the half-life in future experiments. Interestingly, as shown in Fig. 2 that the correlation between ΔP and $|R|$ is not simply linear. Specifically, when the neutron number N_{d} of the daughter nuclei is less than 126, ΔP exhibits a linear relationship with $|R|$; when N_{d} is greater than 126, the two variables still exhibit a linear relationship, but with a steeper slope. This indicates that the correlation between ΔP and $|R|$ is affected by the shell effect, and the decay of daughter nuclei with neutron numbers greater than 126 is more sensitive to the influence of extreme laser fields. Subsequently, to compare the effects of laser fields with different intensities on the cluster penetration probability and half-life, we also calculated the case when the laser intensity is 1×10^{25} W/cm^2. The calculated results are presented in the last two columns of Table 2. The results indicate that an increase in laser intensity by one order of magnitude usually leads to a tripling of the change rate of the penetration probability. This implies that in the future, as the intensity of the laser increases, the half-life of the nucleus will undergo significant changes.

In actual experiments, the direction of cluster emission is random, indicating that the angle between the direction of the laser electric field and that of cluster emission is not consistently zero. In this study, we assumed that the direction of the laser was fixed and that of the emitted cluster was entirely random. To investigate the influence of laser pulses on the cluster penetration probability in any direction, we present the relationship between θ and ΔP for 26 trans-lead nuclei at a peak intensity of 1×10^{24} W/cm^2 in Fig. 3. Here, θ ranges from 0 to π. In this figure, various colored lines represent the variation of ΔP with the angle θ for different cluster emissions. From this figure, it can be seen that the maximum value of ΔP is attained when the direction of the laser electric field is the same as that of

Table 1 Comparisons between the experimental cluster-decay half-lives and the calculated ones using the deformed α-like model

Decay	l	Q_c(MeV)	β_2	β_4	β_6	$\log_{10}T_{1/2}^{exp}$	$\log_{10}T_{1/2}^{cal}$
^{221}Fr→ ^{207}Tl+^{14}C	3	31.32	−0.361	0	0	14.52	14.11
^{221}Ra→ ^{207}Pb+^{14}C	3	32.40	−0.361	0	0	13.39	12.89
^{222}Ra→ ^{208}Pb+^{14}C	0	33.05	−0.361	0	0	11.22	11.45
^{223}Ra→ ^{209}Pb+^{14}C	4	31.83	−0.361	0	0	15.05	14.24
^{224}Ra→ ^{210}Pb+^{14}C	0	30.53	−0.361	0	0	15.86	16.23
^{226}Ra→ ^{212}Pb+^{14}C	0	28.20	−0.361	0	0	21.19	21.19
^{223}Ac→ ^{209}Bi+^{14}C	2	33.06	−0.361	0	0	12.60	12.64
^{225}Ac→ ^{211}Bi+^{14}C	3	30.48	−0.361	0	0	17.34	17.74
^{228}Th→ ^{208}Pb+^{20}O	0	44.72	0.01	−0.024	0.02	20.87	21.42
^{230}U→ ^{208}Pb+^{22}Ne	0	61.39	0.384	0.096	−0.007	19.57	18.22
^{231}Pa→ ^{208}Pb+^{23}F	1	51.84	0.117	0.079	−0.021	26.00	23.80
^{230}Th→ ^{206}Hg+^{24}Ne	0	57.76	−0.063	0.013	−0.03	24.61	23.44
^{231}Pa→ ^{207}Tl+^{24}Ne	1	60.41	−0.063	0.013	−0.03	22.89	21.41
^{232}U→ ^{208}Pb+^{24}Ne	0	62.31	−0.063	0.013	−0.03	20.39	19.60
^{233}U→ ^{209}Pb+^{24}Ne	2	60.49	−0.063	0.013	−0.03	24.82	22.88
^{234}U→ ^{210}Pb+^{24}Ne	0	58.82	−0.063	0.013	−0.03	25.07	24.87
^{235}U→ ^{211}Pb+^{24}Ne	1	57.36	−0.063	0.013	−0.03	27.62	27.77
^{233}U→ ^{208}Pb+^{25}Ne	2	60.70	0.053	0.002	−0.03	24.82	23.32
^{234}U→ ^{208}Pb+^{26}Ne	0	59.47	0.121	−0.052	−0.035	25.25	25.24
^{234}U→ ^{206}Hg+^{28}Mg	0	74.11	0.277	−0.073	0.008	25.53	24.69
^{236}Pu→ ^{208}Pb+^{28}Mg	0	79.67	0.277	−0.073	0.008	21.52	20.74
^{238}Pu→ ^{210}Pb+^{28}Mg	0	75.91	0.277	−0.073	0.008	25.67	25.16
^{236}U→ ^{206}Hg+^{30}Mg	0	72.51	0.119	−0.005	−0.031	27.58	28.35
^{238}Pu→ ^{208}Pb+^{30}Mg	0	76.79	0.119	−0.005	−0.031	25.67	25.35
^{238}Pu→ ^{206}Hg+^{32}Si	0	91.21	−0.124	−0.03	−0.033	25.27	25.27
^{242}Cm → ^{208}Pb+^{34}Si	0	96.54	0	0	−0.039	23.24	23.40

In this table, l denotes the angular momentum carried away by the emitted cluster, Q_c is the decay energy, β_2, β_4, and β_6 are the theoretical quadrupole, hexadecapole, and hexacontatetrapole deformation parameters for the emitted cluster, respectively, mainly taken from Ref. [47]. $T_{1/2}^{exp}$ represents the experimental half-lives from Refs. [23, 26, 46, 59]. $T_{1/2}^{cal}$ denotes the theoretical half-lives of cluster radioactivity given by the adopted model. All the half-lives are in units of seconds, the logarithms of which are presented for the sake of comparison

the emitted cluster (i.e., $\theta = 0$), and the minimum occurs when these two directions are opposite (i.e., $\theta = \pi$). Notably, when $\theta = \pi/2$, ΔP is zero. This implies that the laser field has no impact on the cluster penetration probability when the direction of the laser field is perpendicular to that of the emitted cluster. In addition, one can observe from this figure that ΔP varies with θ similarly for different nuclei at the same laser intensity. When $\theta < \pi/2$, the laser increases the cluster penetration probability; conversely, when $\theta > \pi/2$, the laser decreases this probability. Furthermore, as shown in Fig. 3, the sensitivity of the cluster penetration probability to ultra-intense laser fields appears to be related to the size of the emitted cluster. Specifically, the value range of ΔP in the same cluster emitted by different parent nuclei varies greatly, but the overall range of its value moves approximately linearly upward as the size of the emitted cluster increases.

Interestingly, as shown in Fig. 3, the variation of ΔP with θ seems to be centrally symmetric about $\theta = \pi/2$. This phenomenon spurred our curiosity to explore whether the effects of the laser on the penetration probability at all angles collectively cancel each other out. To verify this, we calculated the average change rate of the cluster penetration probability for $I_0 = 1 \times 10^{24}$ W/cm^2. It is defined as:

$$\Delta P_{\theta_{avg}} = \frac{1}{\pi}\int_0^{\pi} \Delta P(\varepsilon, \theta)\mathrm{d}\theta. \tag{41}$$

The detailed results are presented in Fig. 4. From this figure, it is clear that the $\Delta P_{\theta_{avg}}$ values for the investigated emitters are not equal to 0. This indicates that the promotional and

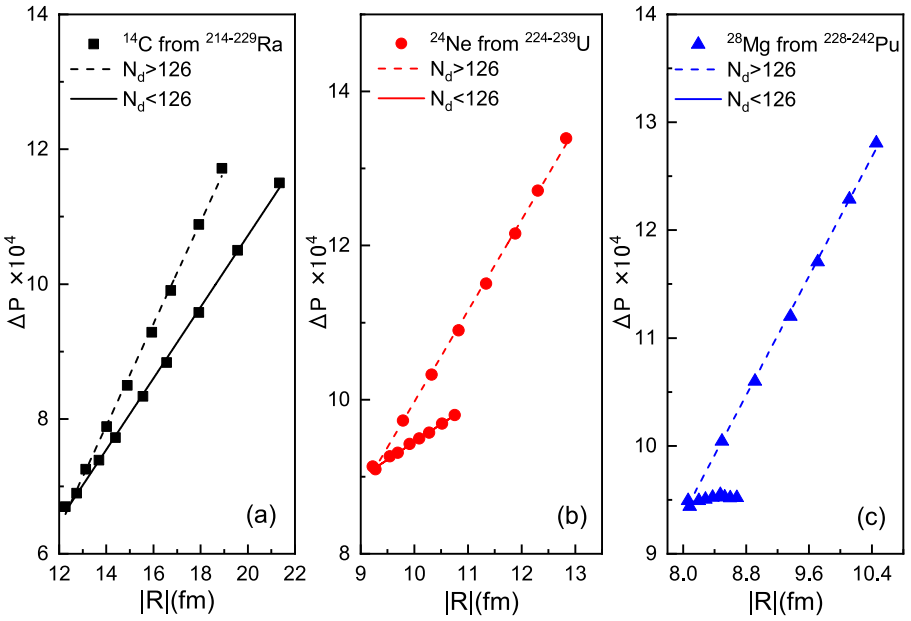

Fig. 2 (Color online) The relationship between the rate of relative change of penetration probability and the average tunneling path length for the emission of clusters ^{14}C, ^{24}Ne and ^{28}Mg, respectively, from Ra, U, Pu isotopes in the case of I_0=1 × 10^{24} W/cm^2.

inhibitory effects of the laser do not completely cancel each other. To further interpret this phenomenon, considering that the laser potential $V_{\rm I}$, which is much smaller than the interaction potential between the emitted cluster and the daughter nucleus, can be regarded as a perturbation to the residual potential $V_{\rm wl} = V_{\rm N} + V_{\rm C} + V_{\rm l} - Q_{\rm c}$, we employed a Taylor series expansion for Eq. (6). It can be given as:

$$\begin{aligned} P(\varepsilon,\theta) &= \exp\left(-\frac{2\sqrt{2\mu}}{\hbar}\int_{R_{\rm in}}^{R_{\rm out}}\sqrt{V_{\rm wl}}\sqrt{1+\frac{V_{\rm I}}{V_{\rm wl}}}{\rm d}r\right) \\ &\approx \exp\left[-\frac{2\sqrt{2\mu}}{\hbar}\int_{R_{\rm in}}^{R_{\rm out}}\left(\sqrt{V_{\rm wl}}\right.\right. \\ &\quad \left.\left.+\frac{V_{\rm I}}{2\sqrt{V_{\rm wl}}}-\frac{V_{\rm I}^2}{8V_{\rm wl}^{3/2}}\right){\rm d}r\right] \\ &= \exp(\chi_0)\exp(\chi_1+\chi_2) \\ &= P(\varepsilon=0)\exp(\chi_1+\chi_2). \end{aligned} \tag{42}$$

Here, χ_0, χ_1, and χ_2 are defined as:

$$\chi_0 = -\frac{2\sqrt{2\mu}}{\hbar}\int_{R_{\rm in}}^{R_{\rm out}}\sqrt{V_{\rm wl}}{\rm d}r, \tag{43}$$

$$\chi_1 = \varepsilon(t)\times\frac{\sqrt{2\mu}Z_{\rm eff}\cos\theta}{\hbar}\int_{R_{\rm in}}^{R_{\rm out}}\frac{r}{\sqrt{V_{\rm wl}}}{\rm d}r, \tag{44}$$

$$\chi_2 = \varepsilon(t)^2\times\frac{\sqrt{2\mu}Z_{\rm eff}^2\cos^2\theta}{4\hbar}\int_{R_{\rm in}}^{R_{\rm out}}\frac{r^2}{V_{\rm wl}^{3/2}}{\rm d}r. \tag{45}$$

Based on Eq. (40), the relative change rate of the cluster penetration probability can be expressed as:

$$\begin{aligned} \Delta P &= \frac{P(\varepsilon=0)\exp(\chi_1+\chi_2)-P(\varepsilon=0)}{P(\varepsilon=0)} \\ &= \exp(\chi_1+\chi_2)-1 \\ &\approx \chi_1+\chi_2. \end{aligned} \tag{46}$$

As shown, χ_1 is proportional to $\cos\theta$ and χ_2 is proportional to $\cos^2\theta$. For intensities at which χ_2 is negligible, the correlation between ΔP and $\cos\theta$ is linear. There is no net gain in the total penetration probability when integrating over all emission directions. However, as the laser intensity increased, the influence of χ_2 became significant. For the rate of change of the total penetration probability integrated over all angles, the linear responses cancel each other out, leaving the quadratic response to dominate. In this case, the $\cos^2\theta$ term, which always makes a positive contribution to $\Delta P_{\theta{\rm avg}}$, causes the impact of the laser field on the penetration probability at all angles to not be offset. This indicates that higher laser intensities are required to alter the total cluster penetration probability integrated over all angles than to modify the penetration probability at a specific angle.

4 Summary

In summary, considering the preformation probability $S_{\rm c}$ and the deformation effect, we systematically investigated the influence of ultra-intense laser fields that can be achieved in the near future on the cluster penetration probability and

Table 2 Comparison of the change rates of cluster penetration probability and half-life under two laser intensities: 1×10^{24} W/cm^2 and 1×10^{25} W/cm^2

Decay	l	Q_c (MeV)	$\|R\|$ (fm)	ΔP^{24}	ΔT^{24}	ΔP^{25}	ΔT^{25}
^{221}Fr→ ^{207}Tl+^{14}C	3	31.32	13.22	7.37×10^{-4}	-7.36×10^{-4}	2.33×10^{-3}	-2.33×10^{-3}
^{221}Ra→ ^{207}Pb+^{14}C	3	32.40	12.74	6.90×10^{-4}	-6.89×10^{-4}	2.18×10^{-3}	-2.18×10^{-3}
^{222}Ra→ ^{208}Pb+^{14}C	0	33.05	12.27	6.70×10^{-4}	-6.69×10^{-4}	2.12×10^{-3}	-2.12×10^{-3}
^{223}Ra→ ^{209}Pb+^{14}C	4	31.83	13.13	7.25×10^{-4}	-7.24×10^{-4}	2.29×10^{-3}	-2.29×10^{-3}
^{224}Ra→ ^{210}Pb+^{14}C	0	30.53	14.02	7.88×10^{-4}	-7.88×10^{-4}	2.49×10^{-3}	-2.49×10^{-3}
^{226}Ra→ ^{212}Pb+^{14}C	0	28.20	15.93	9.28×10^{-4}	-9.27×10^{-4}	2.94×10^{-3}	-2.93×10^{-3}
^{223}Ac→ ^{209}Bi+^{14}C	2	33.06	12.53	6.74×10^{-4}	-6.73×10^{-4}	2.13×10^{-3}	-2.13×10^{-3}
^{225}Ac→ ^{211}Bi+^{14}C	3	30.48	14.36	7.96×10^{-4}	-7.95×10^{-4}	2.52×10^{-3}	-2.51×10^{-3}
^{228}Th→ ^{208}Pb+^{20}O	0	44.72	11.65	8.62×10^{-4}	-8.61×10^{-4}	2.73×10^{-3}	-2.72×10^{-3}
^{230}U→ ^{208}Pb+^{22}Ne	0	61.39	9.89	9.67×10^{-4}	-9.66×10^{-4}	3.06×10^{-4}	-3.05×10^{-3}
^{231}Pa→ ^{208}Pb+^{23}F	1	51.84	10.92	8.93×10^{-4}	-8.93×10^{-4}	2.83×10^{-4}	-2.82×10^{-3}
^{230}Th→ ^{206}Hg+^{24}Ne	0	57.76	10.25	1.04×10^{-3}	-1.04×10^{-3}	3.28×10^{-3}	-3.27×10^{-3}
^{231}Pa→ ^{207}Tl+^{24}Ne	1	60.41	9.60	9.60×10^{-4}	-9.59×10^{-4}	3.04×10^{-3}	-3.03×10^{-3}
^{232}U→ ^{208}Pb+^{24}Ne	0	62.31	9.22	9.13×10^{-4}	-9.12×10^{-4}	2.89×10^{-3}	-2.88×10^{-3}
^{233}U→ ^{209}Pb+^{24}Ne	2	60.49	9.79	9.73×10^{-4}	-9.72×10^{-4}	3.08×10^{-3}	-3.07×10^{-3}
^{234}U→ ^{210}Pb+^{24}Ne	0	58.82	10.33	1.03×10^{-3}	-1.03×10^{-3}	3.27×10^{-3}	-3.26×10^{-3}
^{235}U→ ^{211}Pb+^{24}Ne	1	57.36	10.83	1.09×10^{-3}	-1.09×10^{-3}	3.45×10^{-3}	-3.44×10^{-3}
^{233}U→ ^{208}Pb+^{25}Ne	2	60.70	9.74	9.29×10^{-4}	-9.28×10^{-4}	2.94×10^{-3}	-2.93×10^{-3}
^{234}U→ ^{208}Pb+^{26}Ne	0	59.47	10.14	9.19×10^{-4}	-9.18×10^{-4}	2.91×10^{-3}	-2.90×10^{-3}
^{234}U→ ^{206}Hg+^{28}Mg	0	74.11	8.95	1.07×10^{-3}	-1.07×10^{-3}	3.40×10^{-3}	-3.39×10^{-3}
^{236}Pu→ ^{208}Pb+^{28}Mg	0	79.67	8.06	9.49×10^{-4}	-9.48×10^{-4}	3.00×10^{-4}	-3.00×10^{-3}
^{238}Pu→ ^{210}Pb+^{28}Mg	0	75.91	8.91	1.06×10^{-3}	-1.06×10^{-3}	3.36×10^{-3}	-3.34×10^{-3}
^{236}U→ ^{206}Hg+^{30}Mg	0	72.51	9.17	1.10×10^{-3}	-1.09×10^{-3}	3.49×10^{-3}	-3.48×10^{-3}
^{238}Pu→ ^{208}Pb+^{30}Mg	0	76.79	8.53	9.99×10^{-4}	-9.98×10^{-4}	3.16×10^{-3}	-3.15×10^{-3}
^{238}Pu→ ^{206}Hg+^{32}Si	0	91.21	7.57	1.15×10^{-3}	-1.14×10^{-3}	3.63×10^{-3}	-3.62×10^{-3}
^{242}Cm → ^{208}Pb+^{34}Si	0	96.54	6.96	1.04×10^{-3}	-1.04×10^{-3}	3.29×10^{-3}	-3.28×10^{-3}

In this table, l is the angular momentum carried away by the emitted cluster, Q_c is the decay energy, $|R|$ represents the average tunneling path length. ΔP^{24} and ΔP^{25} are the relative change rates of the cluster penetration probability at intensities of 1×10^{24} W/cm^2 and 1×10^{25} W/cm^2, respectively. ΔT^{24} and ΔT^{25} are the relative change rate of the cluster-decay half-life at an intensity of 1×10^{24} W/cm^2 and 1×10^{25} W/cm^2, respectively

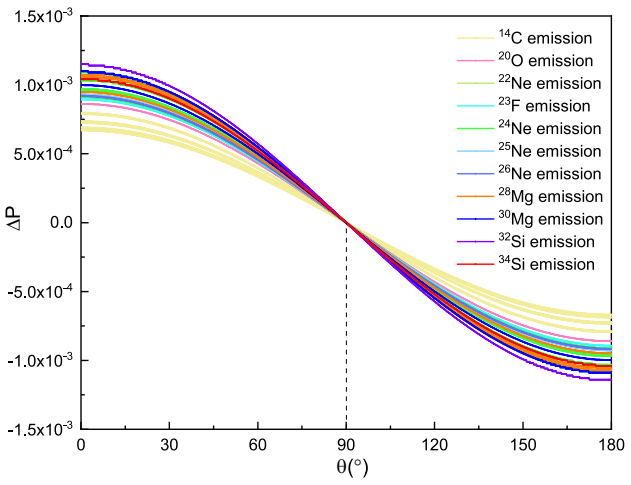

Fig. 3 (Color online) The relationship between ΔP and θ for 26 trans-lead nuclei in the case of $I_0 = 1 \times 10^{24}$ W/cm^2

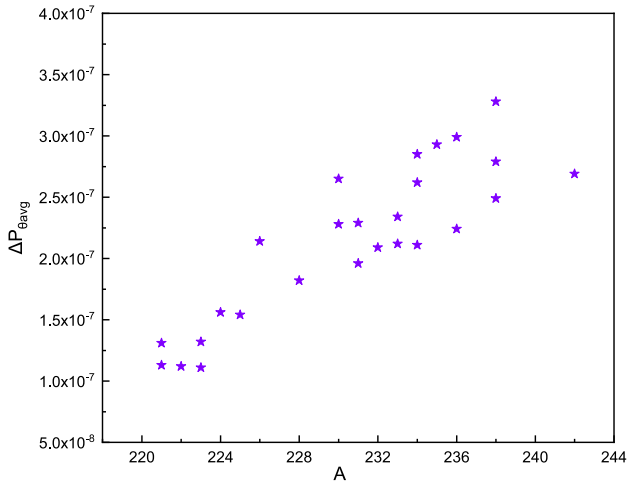

Fig. 4 (Color online) The angle-average change rate of a laser pulse on cluster penetration probability at an intensity of 1×10^{24} W/cm^2

half-life for 26 trans-lead nuclei, aiming to achieve quantitative assessments of the laser's impact on cluster radioactivity and to gain a deeper understanding thereof. The results show that in the environment of extreme laser fields, the changes in the cluster penetration probability and half-life are not significant. However, these slight variations indicate that lasers that can be achieved in the near future are capable of directly affecting nuclear physics, despite the fact that a single laser photon possesses an extremely low energy. Moreover, we discovered that for different parent nuclei emitting the same cluster, nuclei that provide a longer tunneling path are more easily affected by laser fields. The shell effect on the correlation between ΔP and $|R|$ was observed. Next, we discuss the influence of laser fields on the cluster penetration probability in any direction. The total impact of the laser fields on the penetration probability across all angles was also revealed. This can serve as a reference for future theoretical and experimental research on laser–nucleus interactions.

Acknowledgements We would like to thank Dr. S. Luo for the support and helpful discussions.

Author Contributions All authors contributed to the study conception and design. Material preparation, data collection, and analysis were performed by Leng-Jun Liao, Lin-Jing Qi, Xi-Jun Wu, Xiao-Hua Li, and Ming Li. The first draft of the manuscript was written by Leng-Jun Liao, and all authors commented on previous versions of the manuscript. All authors read and approved the final manuscript.

Data Availability The data that support the findings of this study are openly available in Science Data Bank at https://cstr.cn/31253.11.sciencedb.32857 and https://doi.org/10.57760/sciencedb.32857..

Declarations

Conflicts of Interest The authors declare that they have no competing interests.

References

1. T.H. Maiman, Stimulated optical radiation in Ruby. Nature **187**, 493 (1960). https://doi.org/10.1038/187493a0
2. J.W. Yoon, Y.G. Kim, I.W. Choi et al., Realization of laser intensity over 10^{23} W/cm^2. Optica **8**, 630 (2021). https://doi.org/10.1364/OPTICA.420520
3. W. Wang, J. Zhou, B.Q. Liu et al., Exciting the isomeric ^{229}Th nuclear state via laser-driven electron recollision. Phys. Rev. Lett. **127**, 052501 (2021). https://doi.org/10.1103/PhysRevLett.127.052501
4. W.J. Lv, H. Duan, J. Liu, Enhanced deuterium-tritium fusion cross sections in the presence of strong electromagnetic fields. Phys. Rev. C **100**, 064610 (2019). https://doi.org/10.1103/PhysRevC.100.064610
5. S.A. Ghinescu, D.S. Delion, Coupled-channels analysis of the α decay in strong electromagnetic fields. Phys. Rev. C **101**, 044304 (2020). https://doi.org/10.1103/PhysRevC.101.044304
6. Ş Mişicu, M. Rizea, Laser-assisted proton radioactivity of spherical and deformed nuclei. J. Phys. G **46**, 115106 (2019). https://doi.org/10.1088/1361-6471/ab1d7c
7. K.A. Tanaka, K.M. Spohr, D.L. Balabanski et al., Current status and highlights of the ELI-NP research program. Matter Radiat. Extremes **5**, 024402 (2020). https://doi.org/10.1063/1.5093535
8. W.Q. Li, Z.B. Gan, L.H. Yu et al., 339 J high-energy Ti:sapphire chirped-pulse amplifier for 10 PW laser facility. Opt. Lett. **43**, 5681 (2018). https://doi.org/10.1364/OL.43.005681
9. Y. Shvyd'ko, R. Röhlsberger, O. Kocharovskaya et al., Resonant X-ray excitation of the nuclear clock isomer ^{45}Sc. Nature **622**, 471 (2023). https://doi.org/10.1038/s41586-023-06491-w
10. J.T. Qi, H.X. Zhang, X. Wang, Isomeric excitation of ^{229}Th in laser-heated clusters. Phys. Rev. Lett. **130**, 112501 (2023). https://doi.org/10.1103/PhysRevLett.130.112501
11. L. von der Wense, P.V. Bilous, B. Seiferle et al., The theory of direct laser excitation of nuclear transitions. Eur. Phys. J. A **56**, 1 (2020). https://doi.org/10.1140/epja/s10050-020-00177-x
12. Ş Mişicu, M. Rizea, Laser-assisted proton radioactivity of spherical and deformed nuclei. J. Phys. G **46**, 115106 (2019). https://doi.org/10.1088/1361-6471/ab1d7c
13. J.H. Cheng, Y. Li, T.P. Yu, Systematic study of laser-assisted proton radioactivity from deformed nuclei. Phys. Rev. C **105**, 024312 (2022). https://doi.org/10.1103/PhysRevC.105.024312
14. Y.T. Zou, J.H. Cheng, Y.Y. Xu et al., Laser-assisted two-proton radioactivity. J. Phys. G **51**, 045103 (2024). https://doi.org/10.1088/1361-6471/ad2691
15. J.T. Qi, T. Li, R.H. Xu et al., α decay in intense laser fields: calculations using realistic nuclear potentials. Phys. Rev. C **99**, 044610 (2019). https://doi.org/10.1103/PhysRevC.99.044610
16. J.H. Cheng, Q. Xiao, J.G. Deng et al., Laser-assisted α decay of the deformed odd-A nuclei. Nucl. Sci. Tech. **36**, 69 (2025). https://doi.org/10.1007/s41365-024-01610-2
17. A. Pálffy, S.V. Popruzhenko, Can extreme electromagnetic fields accelerate the α decay of nuclei? Phys. Rev. Lett. **124**, 212505 (2020). https://doi.org/10.1103/PhysRevLett.124.212505
18. D.S. Delion, S.A. Ghinescu, Geiger-Nuttall law for nuclei in strong electromagnetic fields. Phys. Rev. Lett. **119**, 202501 (2017). https://doi.org/10.1103/PhysRevLett.119.202501
19. H. Wang, Y.G. Huang, Z.P. Gao et al., α decay and cluster radioactivity in extreme laser fields. Nucl. Sci. Tech. **36**, 169 (2025). https://doi.org/10.1007/s41365-025-01753-w
20. Y.L. Zhang, Y.Z. Wang, Systematic study of cluster radioactivity of superheavy nuclei. Phys. Rev. C **97**, 014318 (2018). https://doi.org/10.1103/PhysRevC.97.014318
21. M. Ismail, W.M. Seif, A. Adel et al., Alpha-decay of deformed superheavy nuclei as a probe of shell closures. Nucl. Phys. A **958**, 202 (2017). https://doi.org/10.1016/j.nuclphysa.2016.11.010
22. W.M. Seif, M. Shalaby, M.F. Alrakshy, Isospin asymmetry dependence of the α spectroscopic factor for heavy nuclei. Phys. Rev. C **84**, 064608 (2011). https://doi.org/10.1103/PhysRevC.84.064608
23. X. Liu, J.D. Jiang, X. Chen et al., Microscopic calculations of nuclear incompressibility from cluster radioactivity. Phys. Rev. C **110**, 034329 (2024). https://doi.org/10.1103/PhysRevC.110.034329
24. X. Liu, J.D. Jiang, X.J. Wu et al., Systematic study of cluster radioactivity in trans-lead nuclei with various versions of proximity potential formalisms. Chin. Phys. C **48**, 054101 (2024). https://doi.org/10.1088/1674-1137/ad260b
25. L.J. Qi, D.M. Zhang, S. Luo et al., Systematic calculations of cluster radioactivity half-lives in trans-lead nuclei. Chin. Phys. C **47**, 014101 (2023). https://doi.org/10.1088/1674-1137/ac94bd
26. L.J. Qi, D.M. Zhang, S. Luo et al., Cluster radioactivity preformation probability of trans-lead nuclei in the N_pN_n scheme. Phys. Rev. C **108**, 014325 (2023). https://doi.org/10.1103/PhysRevC.108.014325

27. Z.Z. Ren, C. Xu, Z.J. Wang, New perspective on complex cluster radioactivity of heavy nuclei. Phys. Rev. C **70**, 034304 (2004). https://doi.org/10.1103/PhysRevC.70.034304
28. A. Sandulescu, D.N. Poenaru, W. Greiner, New type of decay of heavy nuclei intermediate between fission and α decay. Sov. J. Part. Nucl. **11**, 6 (1980)
29. H.J. Rose, G.A. Jones, A new kind of natural radioactivity. Nature **307**, 245 (1984). https://doi.org/10.1038/307245a0
30. D.S. Delion, Universal decay rule for reduced widths. Phys. Rev. C **80**, 024310 (2009). https://doi.org/10.1103/PhysRevC.80.024310
31. P.B. Price, L.M. Cook, A. Markert, Phosphate glasses for identification of heavy ions. Nature **325**, 137 (1987). https://doi.org/10.1038/325137a0
32. M. Balasubramaniam, N.S. Rajeswari, An empirical relation for cluster decay preformation probability. Int. J. Mod. Phys. E **23**, 1450018 (2014). https://doi.org/10.1142/S0218301314500189
33. R. Kumar, M.K. Sharma, Systematic study of various proximity potentials in ^{208}Pb-daughter cluster radioactivity. Phys. Rev. C **85**, 054612 (2012). https://doi.org/10.1103/PhysRevC.85.054612
34. K.P. Santhosh, T.A. Jose, Alpha and cluster decay using modified generalized liquid drop model with iso-spin dependent preformation factor. Nucl. Phys. A **992**, 121626 (2019). https://doi.org/10.1016/j.nuclphysa.2019.121626
35. S.S. Malik, R.K. Gupta, Theory of cluster radioactive decay and of cluster formation in nuclei. Phys. Rev. C **39**, 1992 (1989). https://doi.org/10.1103/PhysRevC.39.1992
36. M. Balasubramaniam, N. Arunachalam, Proton and α-radioactivity of spherical proton emitters. Phys. Rev. C **71**, 014603 (2005). https://doi.org/10.1103/PhysRevC.71.014603
37. K.P. Santhosh, T.A. Jose, Cluster decay half-lives using modified generalized liquid drop model (MGLDM) with different preformation factors. Indian J. Phys. **95**, 121 (2021). https://doi.org/10.1007/s12648-020-01685-8
38. M. Ismail, A.Y. Ellithi, M.M. Selim et al., Semi-analytic calculations of barrier penetration and alpha particle preformation probabilities. J. Phys. G **47**, 055105 (2020). https://doi.org/10.1088/1361-6471/ab7291
39. H.M. Liu, Y.T. Zou, X. Pan et al., Systematic study of cluster radioactivity half-lives based on a modified Gamow-like model. Phys. Scr. **96**, 125322 (2021). https://doi.org/10.1088/1402-4896/ac3dbc
40. S. Kumar, R.K. Gupta, Neck formation and deformation effects in a preformed cluster model of exotic cluster decays. Phys. Rev. C **55**, 218 (1997). https://doi.org/10.1103/PhysRevC.55.218
41. Y.J. Shi, W.J. Swiatecki, Theoretical estimates of the rates of radioactive decay of radium isotopes by ^{14}C emission. Phys. Rev. Lett. **54**, 300 (1985). https://doi.org/10.1103/PhysRevLett.54.300
42. G. Royer, Alpha emission and spontaneous fission through quasi-molecular shapes. J. Phys. G **26**, 1149 (2000). https://doi.org/10.1088/0954-3899/26/8/305
43. M. Ismail, A.Y. Ellithi, M.M. Selim et al., Cluster decay half-lives and preformation probabilities. Phys. Scr. **95**, 075303 (2020). https://doi.org/10.1088/1402-4896/ab8eed
44. M. Wang, W.J. Huang, F.G. Kondev et al., The AME 2020 atomic mass evaluation (II). Tables, graphs and references. Chin. Phys. C **45**, 030003 (2021). https://doi.org/10.1088/1674-1137/abddaf
45. F.G. Kondev, M. Wang, W.J. Huang et al., The NUBASE2020 evaluation of nuclear physics properties. Chin. Phys. C **45**, 030001 (2021)
46. F. Saidi, M.R. Oudih, M. Fellah et al., Cluster decay investigation within a modified Woods-Saxon potential. Mod. Phys. Lett. A **30**, 1550150 (2015). https://doi.org/10.1142/S0217732315501503
47. P. Moller, A.J. Sierk, T. Ichikawa et al., Nuclear ground-state masses and deformations: FRDM (2012). At. Data Nucl. Data Tabl. **109**, 1 (2016). https://doi.org/10.1016/j.adt.2015.10.002
48. C.Y. Wong, Interaction barrier in charged-particle nuclear reactions. Phys. Rev. Lett. **31**, 766 (1973). https://doi.org/10.1103/PhysRevLett.31.766
49. R.K. Gupta, M. Balasubramaniam, R. Kumar et al., Optimum orientations of deformed nuclei for cold synthesis of superheavy elements and the role of higher multipole deformations. J. Phys. G **31**, 631 (2005). https://doi.org/10.1088/0954-3899/31/7/009
50. R. Blendowske, H. Walliser, Systematics of cluster-radioactivity-decay constants as suggested by microscopic calculations. Phys. Rev. Lett. **61**, 1930 (1988). https://doi.org/10.1103/PhysRevLett.61.1930
51. K. Wei, H.F. Zhang, Cluster preformation law for heavy and superheavy nuclei. Phys. Rev. C **96**, 021601 (2017). https://doi.org/10.1103/PhysRevC.96.021601
52. D.M. Deng, Z.Z. Ren, D.D. Ni et al., Realistic α preformation factors of odd-A and odd-odd nuclei within the cluster-formation model. J. Phys. G **42**, 075106 (2015). https://doi.org/10.1088/0954-3899/42/7/075106
53. S.M.S. Ahmed, R. Yahaya, S. Radiman et al., Alpha-cluster preformation factors in alpha decay for even–even heavy nuclei using the cluster-formation model. J. Phys. G **40**, 065105 (2013). https://doi.org/10.1088/0954-3899/40/6/065105
54. J.G. Deng, J.C. Zhao, P.C. Chu et al., Systematic study of α decay of nuclei around the $Z = 82, N = 126$ shell closures within the cluster-formation model and proximity potential 1977 formalism. Phys. Rev. C **97**, 044322 (2018). https://doi.org/10.1103/PhysRevC.97.044322
55. D.M. Deng, Z.Z. Ren, α preformation factors of medium-mass nuclei and the structural effects in the region of crossing the $Z = 82$ shell. Phys. Rev. C **93**, 044326 (2016). https://doi.org/10.1103/PhysRevC.93.044326
56. S.M.S. Ahmed, Alpha-cluster preformation factor within cluster-formation model for odd-A and odd–odd heavy nuclei. Nucl. Phys. A **962**, 103 (2017). https://doi.org/10.1016/j.nuclphysa.2017.03.005
57. D. Mao, Z.W. He, Q. Gao et al., Birefringence-managed normal-dispersion fiber laser delivering energy-tunable chirp-free solitons. Ultr. Sci. **2022**, 9760631 (2022). https://doi.org/10.34133/2022/9760631
58. Ş Mişicu, M. Rizea, α-Decay in ultra-intense laser fields. J. Phys. G **40**, 095101 (2013). https://doi.org/10.1088/0954-3899/40/9/095101
59. M.R. Pahlavani, F. Ahmadvand, Effects of deformation on the cluster and the α-decay half-lives for isotopes of the Trans-lead and the undetected superheavy nuclei. Chin. J. Phys. **90**, 49 (2024). https://doi.org/10.1016/j.cjph.2024.05.007